Multiobjective Optimization of Compensation Networks for Wireless Power Transfer Systems

M. Bertoluzzo, M. Forzan

University of Padova, Department of Industrial Engineering, 35131 Padova, Italy

P. Di Barba, M. E. Mognaschi

University of Pavia, Department of Industrial and Information Engineering, Pavia, 27100, Italy

E. Sieni

University of Insubria, Department of Theoretical and Applied Sciences, Varese, Italy

AbstractPurpose–

Design/methodology/approach–

Findings–

Originality/value–

Keywords

Paper type Research paper

1. Introduction

Wireless Power Transfer Systems (WPTSs) operations rely on the inductive coupling between a transmitting and a receiving coil (H. Feng *et al.*, 2018; R. K. Jha *et al.*, 2018; S. Y. Choi *et al.*, 2015). Suitable Compensation Networks (CNs) are connected to the coils in order to increase the power transferred to the load and the efficiency of the device (Bertoluzzo *et al.*, 2018; H. Feng *et al.*, 2018). In (Bertoluzzo *et al.*, 2020; Bertoluzzo and Sieni, 2019) authors presented automatic methods to design the reactances of generic CNs for automotive applications. In general, a bi-objectives, efficiency and power-to-load, problem is solved. Usually the CNs are designed considering only the nominal supply angular frequency ω_0, however their impedance at higher and lower ω must be much higher in order to filter out the high frequency current harmonics and to prevent the circulation of continuous currents components. The first of these occurrences arises because usually the WPTSs are supplied by a square wave modulated voltage that encompasses all the odd harmonics of the supply frequency; the second derives from the not ideal matching between the amplitude and the duty cycles of the positive and the negative semi periods of the supply voltage. From this background, a many-objective problem arises i.e. maximize the efficiency and the transferred power and maximize the impedance at $\omega_{100}=100\cdot\omega_0$ and $\omega_{0.001}= \omega_0/100$, where ω_{100} and $\omega_{0.01}$ are chosen as representative of the lower and higher frequency bands, respectively. In this paper, in order to solve a many-objective

problem with four objective functions (OFs), an algorithm presented by two of the authors in (Di Barba *et al.*, 2020) is applied. Results were compared with the ones found using a constrained-version of NSGA-II algorithm or the recent many-objective version, NSGA-III (Deb *et al.*, 2002; Deb, 2001; Lahanas *et al.*, 2003; Srinivas and Deb, 1994; K. Deb and H. Jain, 2014).

2. The Many-Objective Problem

Fig. 1 shows the device CNs that connect the coupling inductances L_t and L_{pu}, the WPTS system, to the power supply (left) and to the load (right). The power circuit works at 85 kHz, ω_0, as prescribed by the SAE regulation ("SAE J 2954 Wireless Power Transfer for Light-Duty Plug-in/Electric Vehicles and Alignment Methodology", n.d.). The considered CNs have a T topology at both the sides of the WPTS. In this problem, the CNs are characterized by six degrees of freedom, design variables (X_{1s}, X_{1p}, X_{1t}, X_{2r}, X_{2p}, X_{2L}), i.e the reactances of the network components (Fig. 1).

They can vary in the range [-500; 500] Ω: if the optimal value is positive, an inductance is identified, otherwise it is a capacitance. Four OFs, have been considered: function f_1 is the efficiency of the WPTS, function f_2 is the power transferred to the load [1]. In computing $f_1$and f_2 the inductive reactances are modelled considering their inductance and an equivalent series-connected parasitic resistance (ESR). During the optimization process, the ESRs are adjusted to the inductance values by fixing the quality factor Q at the supply angular frequency ω_0 to the same value that characterizes the coupling inductances.

The objective functions f_3 and f_4 are expressed as:

$$f_3 = Z_{\omega 0}/Z_{\omega 100} \qquad (1)$$

$$f_4 = Z_{\omega 0}/Z_{\omega 0.01} \qquad (2)$$

where $Z_{\omega 0}$ is the impedance seen at the supply inverter output at the nominal supply angular frequency ω_0, and $Z_{\omega 100}$ and $Z_{\omega 0.01}$ are the impedances seen at the angular frequencies ω_{100} and $\omega_{0.001}$.

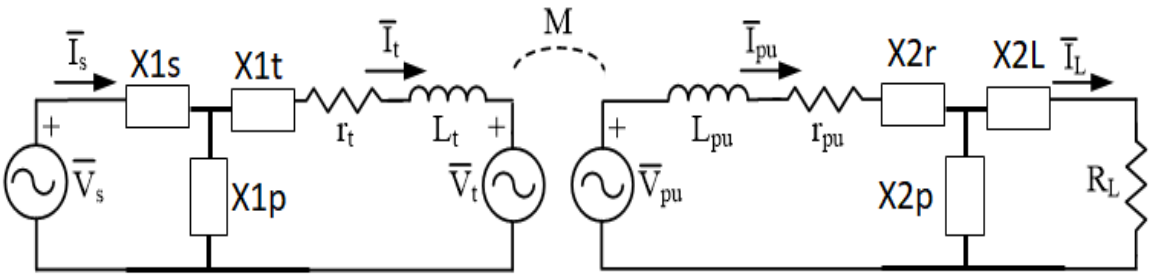

Fig. 1 Scheme of the WPTS with CNs.

The function f_3 and f_4 could also be combined in a f_{34} function in order to reduce the number of the objective functions:

$$f_{34} = f_3 + f_4 = Z_{\omega 0}/Z_{\omega 100} + Z_{\omega 0}/Z_{\omega 0.01} \qquad (3)$$

3. The optimization methods

3.1. The Many-Objective Method

The idea behind this paper is to exploit a single-objective optimization algorithm for minimising a suitable preference function, which takes into account all the objective functions of the optimization problem. The chosen method is EStra, a lowest-order evolutionary algorithm, which has proven to be effective and reliable (Carcangiu *et al.*, 2007; Deb, 2001; Di Barba *et al.*, 2009, 2011; Di Barba and Mognaschi, 2005, 2009; Lahanas *et al.*, 2003; Zitzler and Thiele, 1999).
Traditionally, preference functions are defined as weighted sums of individual objectives and the choice of individual weights is the bias. In contrast, in the proposed method, the aim is to define a weight-free preference function: in view of this, the key idea is the degree of conflict among solutions, because in Pareto-like optimality the non-dominated solutions exhibit the lowest degree of conflict in the set of solutions.
Hence, the road map turns out to be:

- define a preference function, modelling the degree of conflict among objectives, whatever the number of objectives;
- minimise the preference function by means of an evolution strategy algorithm, i.e. a derivative-free and global-optimum oriented algorithm;
- identify a set of least-conflict solutions, approximating a Pareto-optimal set.

The core operation is to compute the degree of conflict between $m \geq 2$ objective functions $(f_1, f_2, \ldots, f_m)$ that are assumed to be simultaneously minimized. After sorting in the ascending order, the rank of a solution is defined as the sorting index of the relevant objective function values.
The computation of the degree of conflict of a solution, called score, is based on the sorting indices of the objective functions; its computing procedure is shown in Fig. 2.
Eventually, the goal is to minimize s with respect to any x in the design space Ω. In view of this, suppose that the preference function s has been linked with a zero-order optimization algorithm: whenever a new candidate solution is created by the algorithm, the set S is expanded by incorporating the (n+1)-th solution (growing set scheme). The whole procedure is repeated up to convergence. For the algorithm to work, an initial set S_0 has to be supplied.

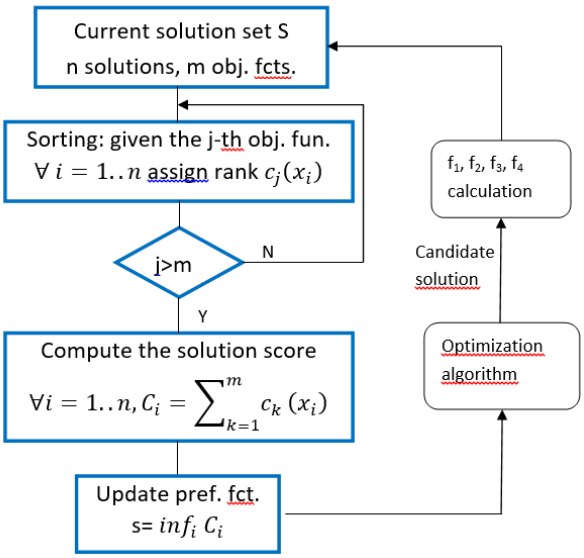

Fig. 2 Block diagram of the many-objective method: the sorting strategy.

It has to be noted that the ranking value assigned to each solution is relevant to the current set S of solutions: whenever a new solution is added to or removed from the set S, the solution score of individual solution has to be recomputed. Hence, the sorting (or ranking) operation of Fig. 2 must be done at each iteration of the optimization, considering the current set of solutions S.

TABLE I STARTING AND FINAL POINTS OF THE OPTIMIZATION: DESIGN VARIABLES AND OBJECTIVE FUNCTION VALUES

	x_1 [Ω] X_{1s}	x_2 [Ω] X_{1p}	x_3 [Ω] X_{1t}	x_4 [Ω] X_{2r}	x_5 [Ω] X_{2p}	x_6 [Ω] X_{2L}
Starting point	-69.7	223	-457	247	427	179
Final point	188	-380	-451	-57.2	-295	-22.4

	f_1	f_2 [W]	f_3	f_4
Starting point	$6.32\ 10^{-4}$	$1.61\ 10^{-8}$	$9.05\ 10^{-2}$	$6.42\ 10^{-2}$
Final point	$4.48\ 10^{-1}$	$7.11\ 10^{-2}$	$1.68\ 10^{-4}$	$1.53\ 10^{-4}$

Specifically, the EStra method, a zero-order optimization algorithm, is chosen. If the method converged, it identifies a single Pareto-optimal solution.

4. Constrained classical bi-objective method

In order to compare the results obtained by the EStra method with a well-known and assessed method, the NSGA-II is applied too. NSGA-II, the classical Non dominated Sorting Genetic Algorithm, developed by Deb (Deb *et al.*, 2002; K. Deb and H. Jain, 2014; Srinivas and Deb, 1994) II can solve bi-objective prob. In this paper NSGA-II was used to optimize the efficiency of the WPTS and the power transferred to the load, f_1 and f_2 respectively, while f_3 and f_4 are considered as constraints as in (Campana *et al.*, 2013). In practice, a threshold level for f_3 and f_4 was set and for all the solutions with f_3 or f_4 larger than the prescribed threshold value, an out-of-range value for f_1 and f_2 is assigned to. In general, f_3 and f_4 is requested to be lower than 1. In the paper the constraint level was fixed between $1.5\ 10^{-4}$ and 1.

5. Optimization Results

The optimization algorithm has been run for 700 iterations. Because EStra is a 1+1 algorithm, one individual is processed at each run. The starting point and the improved solution are shown in Table I.

NSGA-II method was run many times. In particular, the thresholds f_3 and f_4 are subject to, were different for each run: because, in general, the evolutionary algorithms have a poor behavior when constraints are handled, the threshold values have been tightened more and more at each run, in order to make the constraints progressively more severe. In each run, 50 individuals and 250 generations are considered. The results are shown in Fig. 3.

Looking at the results in Fig. 3, it can be noted that the fronts found by NSGA-II are wider when the threshold of the constraints are higher: the lower the constraint values, the narrower the Pareto fronts. When the values are comparable with those obtained by means of the EStra method (let's say the threshold equal to $1.8\ 10^{-4}$), the Pareto front is no longer a front, but all the solutions are grouped closed to a single point in the f_1-f_2 space (pink triangle in Fig. 4).

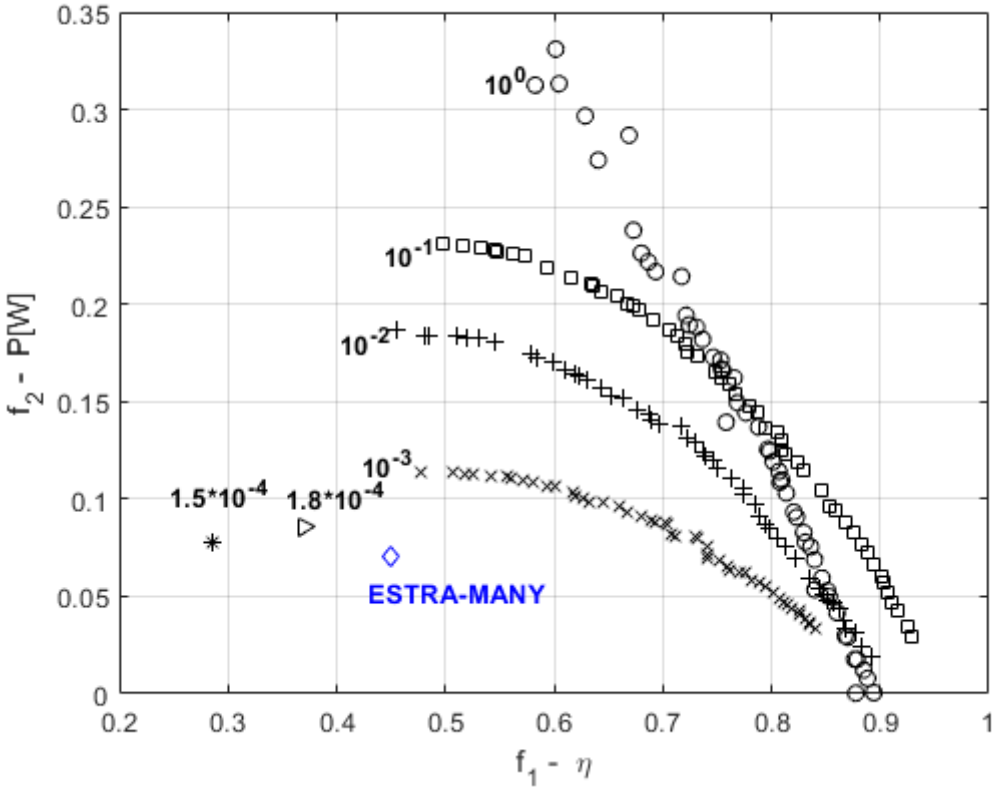

Fig. 3 f_1-f_2 objective function space with results of EStra and NSGA-II methods.

All these solutions are characterized by function f_3 equal to or higher than $1.68\ 10^{-4}$ and f_4 higher than $1.5\ 10^{-4}$. All in one, it can be noted that when the threshold values of f_3 and f_4 are comparable to the relevant values independently found by EStra, then the front recovered by NSGA-II degenerates to a single solution point. The design variables and the values of the objective function f_1 and f_2 reached at the end of the optimization with constraints set to $1.5 \cdot 10^{-4}$ and $1.8 \cdot 10^{-4}$ are listed in Tab. II.

TABLE II FINAL POINTS OF THE NSGA-II OPTIMIZATIONS: DESIGN VARIABLES AND OBJECTIVE FUNCTION VALUES

	x_1 [Ω]	x_2 [Ω]	x_3 [Ω]	x_4 [Ω]	x_5 [Ω]	x_6 [Ω]
NSGA-II $1.5 \cdot 10^{-4}$	122.18	-375.32	-248.76	112.08	-82.62	125.35
NSGA-II $1.8 \cdot 10^{-4}$	119.96	-369.60	-246.21	108.72	-79.30	123.41
		f_1			**f_2 [W]**	
NSGA-II $1.5\ 10^{-4}$		0.286			$7.81\ 10^{-2}$	
NSGA-II $1.8\ 10^{-4}$		0.369			$8.55\ 10^{-2}$	

It can be noted that these solutions are Pareto-indifferent with respect to the EStra solution (black diamond in Fig. 3) because they worsen function f_1 while they are better for function f_2. This is also true if all the four objective functions are considered at a time: for the sake of an example, let's consider solution 1 and solution 2 characterized by k>2 objective functions. It is enough that just one objective function of solution 1 is better than the corresponding objective function of solution 2 and another objective function of solution 1 is worse than the corresponding of solution 2 that the two solutions are Pareto-indifferent. No matter the behavior of the remaining objective functions.

Fig. 3b show the Pareto fronts in Fig. 3 for which the points represented are colored with different colors. Each color represents the value of the function f_3 and f_4 assumed by the represented solution. For instance, if the point in Fig. 3b (a) is green f_3 value is between $1\cdot10^{-2}<f_3<1\cdot10^{-1}$, whereas if it is black $10^{-4}<f_3<1\cdot10^{-3}$. The same colors are used to represent f_4 values in the panel (b).

Table 3 and 4 report the solutions related to constrained NSGA-II optimization considering different constraint levels for f_3 and f_4. The considered levels are $1.5\cdot10^{-4}$, $1.8\cdot10^{-4}$, $1\cdot10^{-3}$, $1\cdot10^{-2}$, $1\cdot10^{-1}$, 1. In particular, it appears that even if the f_3 and f_4 are constrained to be lower than a given level (e.g. 1), in the improved solutions f_3 and f_4 assume a lower level (e.g. close to 10^{-4}). Then also constraining f_3 and f_4 at different level the improved solutions tend to assume lower values. In Table 3 and 4 are reported a selection of improved solutions obtained running NSGA-II with different constraint levels and forcing on the best solution for which f_3 and f_4 are lower than $5\cdot10^{-4}$, respectively.

Table 3 Improved solutions for which $f3<5\cdot10^{-4}$

Constraint level	x1	x2	x3	x4	x5	x6	f1	f2	f3	f4
$1\cdot10^{0}$	40	-56	-182	1	-471	-67	0.73	0.19	$4.8\cdot10^{-4}$	$4.5\cdot10^{-4}$
$1\cdot10^{-1}$	NA									
$1\cdot10^{-2}$	NA									
$1\cdot10^{-3}$	NA									
$1.8\cdot10^{-4}$	120	-370	-246	109	-79	123	0.37	0.09	$1.8\cdot10^{-4}$	$1.5\cdot10^{-4}$
$1.5\cdot10^{-4}$	122	-375	-249	112	-83	125	0.29	0.08	$1.5\cdot10^{-4}$	$1.2\cdot10^{-4}$

Table 4 Improved solutions for which $f4<5\cdot10^{-4}$

Constraint level	x1	x2	x3	x4	x5	x6	f1	f2	f3	f4
$1\cdot10^{0}$	40	-57	-179	0	-470	-66	0.75	0.17	$5.3\cdot10^{-2}$	$5.0\cdot10^{-4}$
$1\cdot10^{-1}$	2	-376	-62	-8	15	-11	0.77	0.15	$1.4\cdot10^{-2}$	$4.7\cdot10^{-4}$
$1\cdot10^{-2}$	23	-226	-100	-86	-349	1	0.75	0.12	$1.4\cdot10^{-3}$	$4.7\cdot10^{-4}$
$1\cdot10^{-3}$	124	-298	-282	-98	-49	18	0.76	0.06	$4.8\cdot10^{-4}$	$4.1\cdot10^{-4}$
$1.8\cdot10^{-4}$	120	-370	-246	109	-79	123	0.37	0.09	$1.8\cdot10^{-4}$	$1.5\cdot10^{-4}$
$1.5\cdot10^{-4}$	122	-375	-249	112	-83	125	0.29	0.08	$1.5\cdot10^{-4}$	$1.2\cdot10^{-4}$

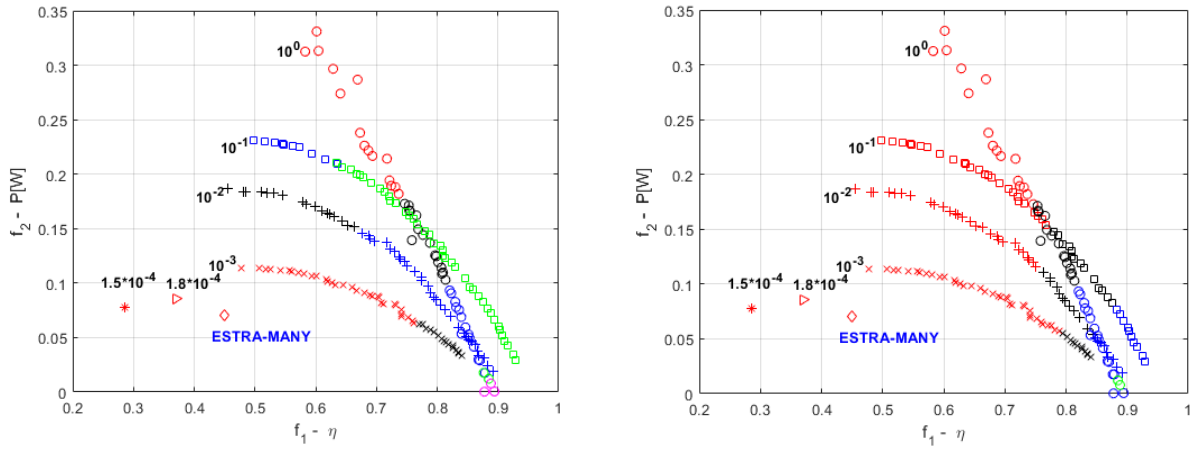

Fig. 3b f_1-f_2 objective function space with results of EStra and NSGA-II methods. Different colors identify the interval value at which belong the value of the f_3 and f_4. Magenta, $1\cdot10^{-1}<f_3, f_4<1\cdot10^{0}$, green $1\cdot10^{-2}<f_3, f_4<1\cdot10^{-1}$, blue$1\cdot10^{-3}<f_3, f_4<1\cdot10^{-2}$, black $5\cdot10^{-4}<f_3, f_4<1\cdot10^{-3}$and red $f_3, f_4<5\cdot10^{-3}$ f_3

Table 5 reports a set of improved solutions for which the focus is based on the trad-off of f_1 and f_2 objective. The proposed solutions were evaluated using NSGA-II algorithm with different constraint levels. It appears, that the chosen solutions show higher value for f_1 and f_2 maintaining a lower value for f_3 and f_4.

Table 3 Improved solutions for which $f4<5\cdot10^{-4}$

Constraint level	x1	x2	x3	x4	x5	x6	f1	f2	f3	f4
$1\cdot10^{0}$	40	-69	-141	-5	-470	-66	0.86	0.04	2.6E-03	2.2E-03
$1\cdot10^{-1}$	1	-373	-62	-14	27	-18	0.88	0.08	5.5E-02	1.1E-03
$1\cdot10^{-2}$	23	-314	-106	-81	-349	5	0.85	0.05	3.7E-03	1.1E-03
$1\cdot10^{-3}$	122	-287	-282	-78	-49	10	0.83	0.04	7.9E-04	6.8E-04
$1.8\cdot10^{-4}$	120	-370	-246	109	-79	123	0.37	0.09	1.8E-04	1.5E-04
$1.5\cdot10^{-4}$	122	-375	-249	112	-83	125	0.29	0.08	1.5E-04	1.2E-04

6. Performance of the Optimized CNs

The magnitude Bode diagram of the frequency response of the impedance $\overline{Z}_s$ seen by the supply generator (see Fig. 1) is shown in Fig. 4.
The red plot refers to the optimized solution obtained by EStra and characterized by the reactances listed in Tab. I. The dashed blue and green plots are relevant to the optimized solutions reported in Tab. II and computed by NSGA-II. The parameters of the inductances and the equivalent load R_L used in computing the objective functions are reported in Tab. 6. They are taken from a prototypal low-power WPTS (G. Buja *et al.*, 2015).

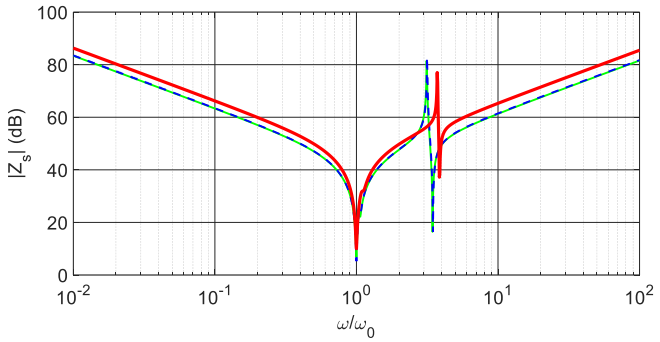

Fig. 4 Magnitude Bode diagram of Z_s vs. ω/ω_0 relevant to the optimized solutions.

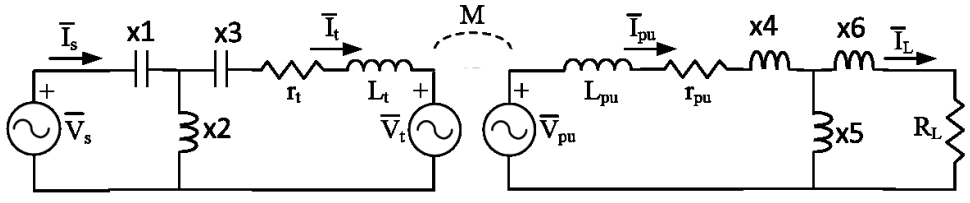

Fig. Obtained CNs with ESTRA-MANY algorithm

Analysis of the plots shows that both the optimization methods successfully prevent the flowing of unwanted current components in the supply inverter and in the transmitting CN. Indeed, for EStra the ratios $Z_{\omega 0}/Z_{\omega 100}$ and $Z_{\omega 0}/Z_{\omega 0.01}$ are 75.5 dB and 72.9 dB, respectively while for both the Bode diagrams relevant to NSGA-II the ratios are 76.5 dB and 74.8 dB.

The Bode diagrams have a pair of marked resonant and anti-resonant peaks at frequencies between three and four times the supply one. From this point of view, EStra provides better results than NSGA-II because the spurious resonance peaks have lower amplitude and are located at frequencies further away from the third harmonic of ω_0. Therefore, it is less likely that the resonance peaks affect the current of the supply inverter even if it generates a square wave voltage with frequency a little higher than the nominal one. More precisely, the peak of minimum impedance coming from EStra is set at a normalized frequency of 3.85 and has a magnitude of 37.19 dB while both the peaks coming from NSGA-II are set at a normalized frequency of 3.47 and their magnitude is 16.45 dB, so that corresponding impedance is about 10 times lower than that obtained with EStra.

At frequencies a little higher than the supply one the Bode diagrams of the impedance exhibit a small distortion, as shown in the magnification reported in Fig. 5. Also in this case, the solution coming from EStra performs better than the other two because the distortion is smaller and happens at an angular frequency further away from the supply one.

A second verification of the optimization performance of EStra has been carried out by simulating the circuit of Fig. 1 in the Simulink environment. The ability of the optimized CNs to reject both high and low frequency components has been checked by supplying the circuit with a square-wave voltage with an offset equal to the voltage amplitude. The plot of the supply voltage is shown in the upper half of Fig. 6. The waveform of the corresponding supply current is reported in the lower half of the same figure.

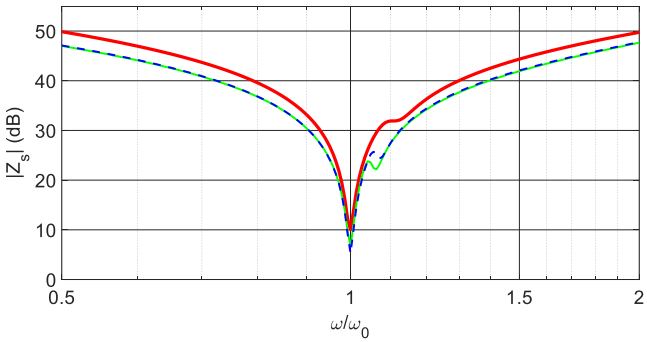

Fig. 5 Magnification of the magnitude Bode diagram of Z_s vs. ω/ω_0 relevant to the optimized solutions.

TABLE 6 PARAMETERS OF THE COUPLING INDUCTANCES

L_t	120 μH
L_{pu}	120 μH
M	30 μH
Q	130
R_L	5.6 Ω

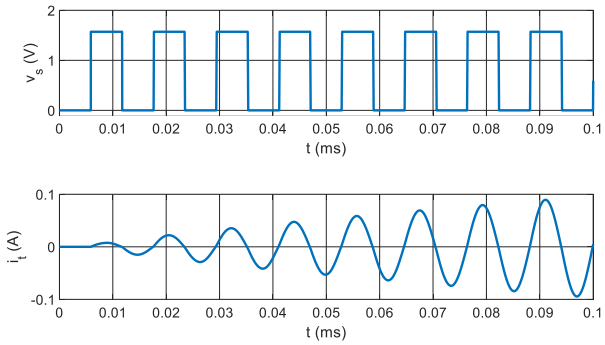

Fig. 6 Supply voltage (upper half) and supply current (lower half) during the first functioning periods.

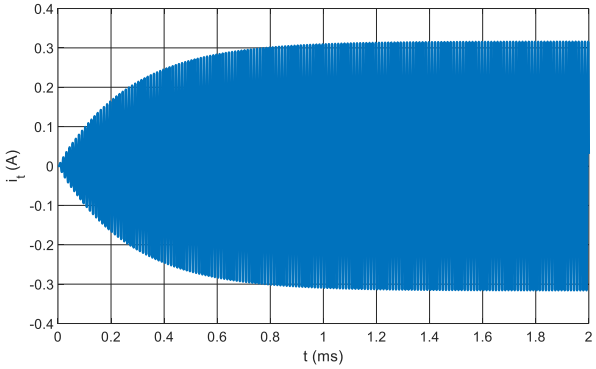

Fig. 7 Supply voltage (upper half) and supply current (lower half) from turning on to steady state.

It clearly appears that the current does not exhibit any continuous component and that it is slightly distorted only in the very first supply periods while any harmonics disappear after a very short time interval. Figure 7 demonstrates that despite the sudden application of the supply voltage, the current reaches smoothly its steady state condition, without discontinuities or undue oscillations of its amplitude.

7. Conclusions

The comparison of the values taken by the OFs before and after the optimization shows that the EStra algorithm effectively enhanced the performance of the CNs and their impedance to the unwanted current harmonics, as confirmed by the magnitude Bode diagram of Fig. 4 and by the results coming from the simulations reported in Fig. 6 and 7.

References

Bertoluzzo, M., Forato, M. and Sieni, E. (2018), "Optimization of the Compensation Networks for WPT Systems", *IECON 2018 - 44th Annual Conference of the IEEE Industrial Electronics Society*, IEEE, Washington, DC, pp. 4828–4833.

Bertoluzzo, M., Giacomuzzi, S. and Sieni, E. (2020), "Automatic Optimization of the Compensation Networks of a Wireless Power Transfer System", *Energies*, Vol. 13 No. 20, p. 5298.

Bertoluzzo, M. and Sieni, E. (2019), "Optimal design of the compensation networks of an inductive wireless power transfer system", *COMPEL - The International Journal for Computation and Mathematics in Electrical and Electronic Engineering*, Vol. ahead-of-print No. ahead-of-print, available at:https://doi.org/10.1108/COMPEL-06-2019-0262.

Campana, L.G., Di Barba, P., Dughiero, F., Rossi, C.R. and Sieni, E. (2013), "Optimal Needle Positioning for Electrochemotherapy: A Constrained Multiobjective Strategy", *IEEE Transactions on Magnetics*, Vol. 49 No. 5, pp. 2141–2144.

Carcangiu, S., Di Barba, P., Fanni, A., Mognaschi, M.E. and Montisci, A. (2007), "Comparison of multi-objective optimisation approaches for inverse magnetostatic problems", edited by Martone, R.*COMPEL - The International Journal for Computation and Mathematics in Electrical and Electronic Engineering*, Vol. 26 No. 2, pp. 293–305.

Deb, K. (2001), *Multi-Objective Optimization Using Evolutionary Algorithms*, 1st ed., John Wiley & Sons, Chichester ; New York.

Deb, K., Pratap, A., Agarwal, S. and Meyarivan, T. (2002), "A fast and elitist multiobjective genetic algorithm: NSGA-II", *Evolutionary Computation, IEEE Transactions On*, Vol. 6 No. 2, pp. 182–197.

Di Barba, P., May, H., Mognaschi, M.E., Palka, R. and Savini, A. (2009), "Multiobjective design optimization of an excitation arrangement used in superconducting magnetic bearings", *International Journal of Applied Electromagnetics and Mechanics*, Vol. 30 No. 3–4, pp. 127–134.

Di Barba, P. and Mognaschi, M.E. (2005), "Recent experiences of multiobjective optimisation in electromagnetics: A comparison of methods", *COMPEL - The International Journal for Computation and Mathematics in Electrical and Electronic Engineering*, Vol. 24 No. 3, pp. 921–930.

Di Barba, P. and Mognaschi, M.E. (2009), "Industrial Design With Multiple Criteria: Shape Optimization of a Permanent-Magnet Generator", *IEEE Transactions on Magnetics*, Vol. 45 No. 3, pp. 1482–1485.

Di Barba, P., Mognaschi, M.E., Palka, R., Savini, A. and Yatchev, I. (2011), "Automated optimal design of a HTS coreless winding", *International Journal of Applied Electromagnetics and Mechanics*, Vol. 37 No. 2–3, pp. 93–99.

Di Barba, P., Mognaschi, M.E. and Wiak, S. (2020), “A non-differential method for solving many-objective optimization problems: An application in IPM motor design”, *International Journal of Applied Electromagnetics and Mechanics*, Vol. Preprint No. Preprint, pp. 1–12.

G. Buja, M. Bertoluzzo and K. N. Mude. (2015), “Design and Experimentation of WPT Charger for Electric City Car”, *IEEE Transactions on Industrial Electronics*, Vol. 62 No. 12, pp. 7436–7447.

H. Feng, T. Cai, S. Duan, X. Zhang, H. Hu and J. Niu. (2018), “A Dual-Side-Detuned Series–Series Compensated Resonant Converter for Wide Charging Region in a Wireless Power Transfer System”, *IEEE Transactions on Industrial Electronics*, Vol. 65 No. 3, pp. 2177–2188.

K. Deb and H. Jain. (2014), “An Evolutionary Many-Objective Optimization Algorithm Using Reference-Point-Based Nondominated Sorting Approach, Part I: Solving Problems With Box Constraints”, *IEEE Transactions on Evolutionary Computation*, Vol. 18 No. 4, pp. 577–601.

Lahanas, M., Schreibmann, E., Milickovic, N. and Baltas, D. (2003), “Evolutionary Multi-Criterion Optimization”, Vol. 2632, Springer Berlin / Heidelberg, p. 70.

R. K. Jha, G. Buja, M. Bertoluzzo, S. Giacomuzzi and K. N. Mude. (2018), “Performance Comparison of the One-Element Resonant EV Wireless Battery Chargers”, *IEEE Transactions on Industry Applications*, Vol. 54 No. 3, pp. 2471–2482.

S. Y. Choi, B. W. Gu, S. Y. Jeong and C. T. Rim. (2015), “Advances in Wireless Power Transfer Systems for Roadway-Powered Electric Vehicles”, *IEEE Journal of Emerging and Selected Topics in Power Electronics*, Vol. 3 No. 1, pp. 18–36.

“SAE J 2954 Wireless Power Transfer for Light-Duty Plug-in/Electric Vehicles and Alignment Methodology”. (n.d.). , SAE, available at: https://www.sae.org/standards/content/j2954_201605/.

Srinivas, N. and Deb, K. (1994), “Multiobjective optimization using nondominated sorting in genetic algorithms”, *Evolutionary Computation*, Vol. 2, pp. 221–248.

Zitzler, E. and Thiele, L. (1999), “Multiobjective evolutionary algorithms: a comparative case study and the strength Pareto approach”, *Evolutionary Computation, IEEE Transactions On*, Vol. 3 No. 4, pp. 257–271.